# CRDS measurements of air-broadened lines in the 1.6 $\mu$m band of 12CO2 : Line shape parameters with their temperature dependence

Didier Mondelain, A. Campargue, H. Fleurbaey, S. Kassi, S. Vasilchenko

# CRDS measurements of air-broadened lines in the 1.6 µm band of $^{12}CO_2$: Line shape parameters with their temperature dependence

D. Mondelain*, A. Campargue, H. Fleurbaey, S. Kassi, S. Vasilchenko

*Univ. Grenoble Alpes, CNRS, LIPhy, 38000 Grenoble, France*

*Corresponding author: didier.mondelain@univ-grenoble-alpes.fr; LIPhy, Bat. E, 140 rue de la Physique, 38400 Saint-Martin d'Hères (France).

**Key words**

Line shape; carbon dioxide; temperature dependence; CRDS

**Abstract**

The $^{12}CO_2$ band at 1.6 µm is used for carbon dioxide monitoring in the Earth atmosphere. The targeted accuracy of these measurements motivates important efforts to improve the quality of the spectroscopic parameters in atmospheric conditions. In the present work, the line shapes of the R(6), R(12), R(16), R(18) and R(20) transitions of the 30013-00001 band of $^{12}CO_2$ in air are studied with a cavity ring down spectrometer (CRDS). For each transition, high signal-to-noise ratio spectra (between 2000 and 20000) are recorded at different temperatures (250, 274, 285, 295 and 320 K) and total pressures (50, 100, 250, 500 and 750 Torr). To this end, a spectrally narrowed and stable (sub-kHz) laser source is coupled into a temperature regulated high-finesse optical cavity. The frequency scale of each spectrum is accurately determined from measurements of the frequency of the beat note between a part of the laser light and the closest tooth of a frequency comb referenced to a rubidium clock. A multi-spectrum fit procedure with quadratic speed dependent Nelkin-Ghatak profiles, including line-mixing effects, has been used to derive for each transition, the different spectroscopic parameters and their temperature dependence. Results are discussed in comparison with previous experimental data, HITRAN2020 database and values obtained from requantized classical molecular dynamics simulations (rCMDS).

## 1. Introduction

Due to its importance for remote sensing applications from ground- or satellite-based observatories, the 30013-00001 band of $^{12}CO_2$ in the 1.6 µm atmospheric transparency window has been the subject of many laboratory studies using Fourier transform spectroscopy (FTS) [1,2 and references herein] and cavity ring down spectroscopy (CRDS) [3,4,5,6,7]. This band is especially used to monitor the column averaged $CO_2$ atmospheric dry air mole fraction, $X_{CO2}$, in several satellite missions like the Orbiting Carbon Observatory-2 (OCO-2) [8,9,10], OCO-3 [11] and GOSAT [12]. A relative uncertainty of less than 0.3 % (*i.e.* ~1 ppm) is required [13] to better characterize the surface $CO_2$ sources and sinks on regional scales and constrain the climate models. This brings strong quality constrains on the spectroscopic parameters which have to be determined with very small uncertainties. As stated in [14], *the spectroscopic error estimates (…) are generally comparable to or larger than the noise-only $X_{CO2}$ posterior uncertainty (…)*, showing the importance of new experimental data with improved accuracy. Moreover, upcoming missions like CO2M [15] will have even stronger requirements on $X_{CO2}$ and thus on the spectroscopic parameters and their temperature dependence. In parallel, it is necessary to make available accurate spectroscopic line-shape parameters for $CO_2$ lines to improve the semi-empirical models used to update all of the carbon dioxide transitions in the spectroscopic databases (*e.g.* HITRAN [16] or GEISA [17]), especially for the non-Voigt parameters [18]. The same accurate experimental data are also valuable for validation tests of the parameters provided by requantized classical molecular dynamics simulations (rCMDS) [19].

The aim of this work is to determine the line-shape parameters and their temperature dependence with a reduced uncertainty for five transitions belonging to the R-branch of the 30013-00001 band of $^{12}CO_2$ in air. To achieve this goal, parameters are retrieved from high signal-to-noise ratio CRDS spectra recorded at different temperature and pressure conditions with a spectrally narrowed and stable (sub-kHz) laser source coupled into a temperature regulated high-finesse optical cavity. The frequency scale of each spectrum is accurately determined from measurements of the frequency of the beat note between a part of the laser light and the closest tooth of a frequency comb referenced to a rubidium clock. The experimental set-up is described in Part 2 together with the recording procedure. The multi-spectrum fit procedure and the retrieved spectroscopic parameters are detailed in Part 3. The latter are compared with the most recent and accurate experimental and theoretical data in Part 4 before concluding (Part 5).

## 2. Experimental details

### *2.1 The setup*

The comb-referenced cavity ring down spectrometer used for the recordings has been detailed in [20] and is only briefly described here. The light source consists in a distributed feedback (DFB) laser diode narrowed to sub-kHz level thanks to an optical feedback signal from a stable V-shape high finesse cavity (FSR= 480 MHz; finesse= 500000) made of ultra-low expansion glass [21]. At the same time, the optical feedback allows locking the laser diode to one of the longitudinal cavity modes. The continuous tuning of the light source is achieved thanks to a Mach-Zehnder modulator (MZM) generating a side-band scanned between 2 GHz and 22 GHz from the carrier frequency (*i.e.* over 0.67 $cm^{-1}$). By locking the laser diode to different cavity modes and changing the side band frequency, a continuous tuning is achieved between 6231.5 $cm^{-1}$ and 6243.5 $cm^{-1}$ with the DFB diode at disposal (From Fitel). Due to the low efficiency (~5%) of the MZM, the output beam is amplified by a booster optical amplifier (BOA) before being separated in three parts: towards the high finesse cavity, the wavelength meter (HighFinesse WSU7-IR) and the frequency comb (Model FC 1500-250 WG from Menlo Systems) .

Most of the light is coupled into a temperature stabilized high finesse cavity (TS-HFC) described in [22] where ring down (RD) events are achieved at resonance by switching the laser light off with an acousto-optic modulator (AOM). The extinction coefficient, $\alpha(\nu)$, is deduced from:

$$\alpha(\nu) = \frac{n}{c\tau(\nu)} - \frac{1}{c\tau_0(\nu)} \quad (1)$$

where $\tau$ and $\tau_0$ are the RD times for the cell filled with the gas mixture and evacuated, respectively, $c$ is the speed of light and $n$ is the refractive index of the absorbing gas. RD events are acquired at a typical rate of 200 RD/s by applying a triangular voltage ramp coupled to a RD tracking loop on the PZT tube on which the output cavity mirror is mounted [20].

Accurate measurement of the absolute frequency of the laser source is deduced at each RD event from the frequency of the beat note, $f_{BN}$, between a part of the light source and one tooth of a frequency comb (FC) [20]. The comb tooth number is determined from the wavelength meter measurements.

Two versions of the TS-HFC, described in [20] and [22], are used here, namely the V1 (FSR= 258 MHz; $F$~ 211600) and the improved V2 (FSR= 332 MHz; $F$~ 310600) versions. Both work on the same principle (see Fig.1 of Ref. [22]): a fluid, whose temperature is regulated using a deported refrigerated/heating circulator (model Corio 1000F from Julabo), flows through two counter-propagating copper coils wrapped around a tube containing the two dielectric mirrors of the cavity. An inner copper tube is placed between the mirrors to limit the convection and reduce exchange of the gas inside the tube with the surrounding gas. It has been shown that the surrounded gas is very

well thermalized to the tube temperature (with a difference smaller than 0.05°C) [20]. The latter is measured by four 3-wires 1000 Ω platinum temperature sensors (⅓ DIN class B; accuracy: ±0.1 K to 0.2 K) for the V1 cell and by five 4-wires 100 Ω platinum temperature sensors (class 1/10 DIN) giving an accuracy equal to 0.03+0.0005*t* (with *t* the temperature in °C) for the V2 cell. In both versions, the gas temperature can be regulated over the 245-330 K range, with a maximal temperature variation along the inner tube, $\Delta T$, of 0.5 K and 0.1 K for the for the V1 and V2 cell, respectively. The former one was used for spectra recordings at room temperature and 274 K, where $\Delta T$ is kept below 0.3 K, and the latter one at 320, 285 and 250 K (**Table 1**). The temperature variations are limited to only 0.04 K over ~14h at 250 K.

A gas mixture of 398.9±2.0 (2σ) mol-ppm of $CO_2$ in air (Ar: ~1 mol-% ; $O_2$: ~20.95 mol-%; $N_2$: ~ 78.05 mol-%) provided by AirLiquide is used in this work. The pressure in the cells is measured by a heated absolute Baratron capacitance manometer (1000 mbar full scale; accuracy: 0.10% of reading).

| 30013-00001 | $\nu_0$ $cm^{-1}$ | *S(296 K)* cm/mol | 320K | 295K | 285K | 274K | 250K |
|---|---|---|---|---|---|---|---|
| **R(6)** | 6233.183 | $1.097\times10^{-23}$ | V2 | V1 | V2 | V1 | V2 |
| **R(12)** | 6237.421 | $1.656\times10^{-23}$ | V2 | V1 | V2 | V1 | V2 |
| **R(16)** | 6240.104 | $1.751\times10^{-23}$ | V2 | V1 | V2 | V1 | V2 |
| **R(18)** | 6241.403 | $1.721\times10^{-23}$ | V2 | V1 | V2 | V1 | V2 |
| **R(20)** | 6242.672 | $1.646\times10^{-23}$ | V2 | V1 | V2 | V1 | V2 |

*Table 1. Summary of the temperature conditions and cell version used to record the five $CO_2$ transitions studied in this work. Position and intensity values are those provided in the HITRAN database [16].*

*2.2. Spectra acquisition*

For each transition and temperature conditions reported in **Table 1**, a series of spectra are recorded for five total pressure values (750, 500, 250, 100 and 50 Torr). With the V1 cell, one spectrum was recorded for each pressure with a sampling step corresponding to the FSR of the cavity (*i.e.* 0.0087 $cm^{-1}$). The spectral sampling corresponding to the FSR of the cavity is adopted to increase the efficiency of the RD tracking loop (reducing the acquisition time) as the resonance always occurs at the same offset value of the ramp. With V2, the recording procedure was modified to provide more measurement points: at each pressure, four spectra were recorded for the absorption line from the starting frequency, $f_{start}$, for the first one and from $f_{start}$ shifted by ¼, ½ and ¾ of the FSR value for the others (**Figure 1**). The acquisition time of one spectrum is typically 1 to 2 minutes. It is important to mention that as the $CO_2$ concentration can slightly evolve with time due to adsorption or desorption on the walls of the cell, it is a better choice to not concatenate the spectra recorded at a given pressure but fit them separately during the multi-spectrum fitting procedure described below. In this way, the evolution of the concentration over one spectrum can be considered as negligible

(0.1% in the worst case). Note that the adsorption or desorption rate depends on the temperature and pressure conditions.

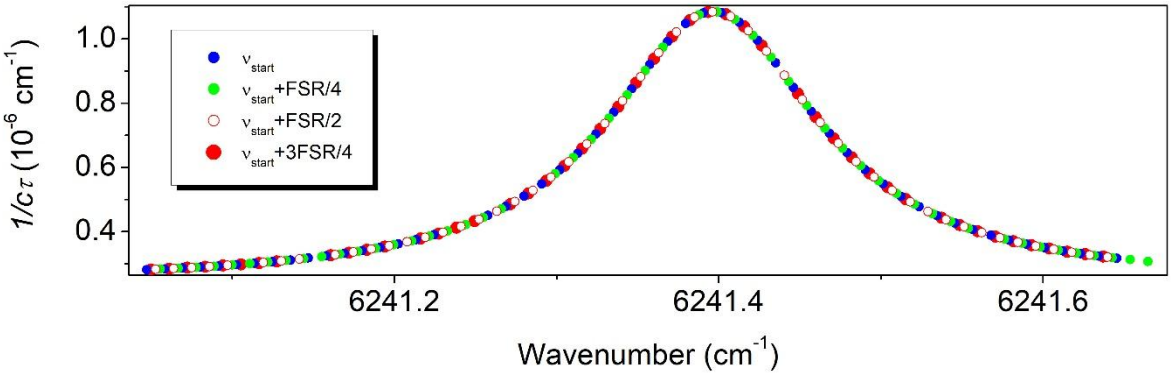


*Figure 1. The spectral sampling applied during the spectra recordings with V2 of the TS-HFC illustrated here for the R(18) transition at 750 Torr and 250 K with the $CO_2$ in air mixture. The different colors correspond to the four interlaced spectra.*

During the spectra recordings, an adaptative averaging procedure is applied to compensate the noise level increase occurring at strong absorption near the center of the lines. This consists in automatically increasing the number of RDs averaged per spectral point with absorption until a user defined maximum value (in order to avoid too long acquisition times). Typically, 50 and 250 RD events are averaged in the wings and at the top of the absorption line, respectively.

## 3. Line profile analysis

### *3.1. The multi-spectrum fit procedure*

The same fit procedure is adopted for all the transitions: at a given temperature the five (V1 cell) or twenty spectra (corresponding to the four interlaced spectra times the five pressures in the case of the V2 cell) are taken into account in a multi-spectrum fit procedure using the *Multi-spectrum Analysis Tool for Spectroscopy (MATS)* fitting program [23] developed at NIST. As illustrated in **Figure 2**. Large residuals are obtained if the speed dependent Voigt profile is used. A better spectra reproduction is achieved by adding line-mixing effects but to reduce residuals at the noise level, it is necessary to use a speed-dependent Nelkin-Ghatak profile (SDNGP) [24] including first-order line mixing [25]. Note that the first-order approximation adopted in our work is valid if the off-diagonal relaxation matrix element coefficients times the pressure is much smaller than the difference between the positions of the neighbor lines [18]. This condition is verified in our case with matrix element coefficients smaller than 0.025 $cm^{-1}atm^{-1}$ [1] and differences in position on the order of ~1.3 $cm^{-1}$ and maximum pressure values of 1 atm. The SDNG profile takes into account the Doppler effect, the collision-induced velocity changes, quantified by the velocity changing collision rate (in $cm^{-1}$), $\nu_{VC}$, the collisional broadening and shift for which a quadratic law is used for the speed dependence such that:

$$\Gamma(v) = \Gamma_0 + \Gamma_2\left[\left(\frac{v}{\tilde{v}}\right)^2 - 3/2\right] \quad (2)$$

and

$$\Delta(v) = \Delta_0 + \Delta_2\left[\left(\frac{v}{\tilde{v}}\right)^2 - 3/2\right] \quad (3)$$

where $\Gamma_0$ and $\Delta_0$ (in $cm^{-1}$) correspond to the (thermally averaged) line width and shift, respectively, and $\Gamma_2$ and $\Delta_2$ (in $cm^{-1}$) are the speed dependence components. $\tilde{v} = \sqrt{\frac{2k_BT}{m}}$ is the most probable speed of the absorbing molecule ($^{12}C^{16}O_2$) of mass $m$. The first-order line mixing is characterized by the dimensionless $Y$ parameter. Note that when fitting the correlation parameter, $\eta$, with a Hartmann Tran profile (HTP), the retrieved value is close to 0 and does not improve the fit quality. Thus, to avoid the risk of a overfitting of the spectra [26], we decided to fix $\eta$ to 0 corresponding to a SDNG profile.

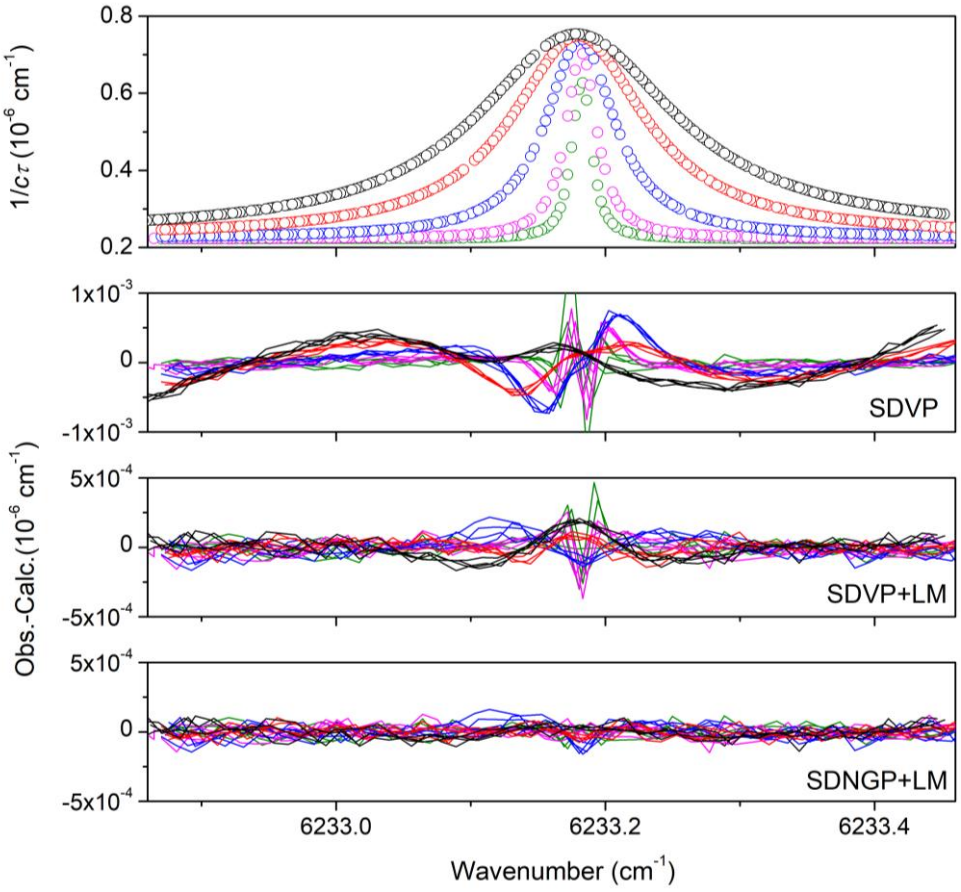


*Figure 2. Series of CRDS spectra recorded for the R(6) transition at 250 K for five pressures between 50 and 750 Torr (upper panel). Corresponding fit residuals (exp-fit) obtained after the multi-spectrum fit procedure with different line profiles are shown on the lower panels. The different colors correspond to the different pressures. For each pressure value, the residuals of the four interlaced spectra are displayed. The quality factors vary between 7700 and 14300 according to the spectrum in the case of SDNGP+LM. Note the different y-scales on the residuals.*

In the multi-spectrum fit procedure, the wavenumber of the spectral line at zero pressure, $\nu_0$, the line-broadening and pressure-shift coefficients $\gamma_0$ ($\Gamma_0/P$, in $cm^{-1}atm^{-1}$) and $\delta_0$ ($\Delta_0/P$, in $cm^{-1}atm^{-1}$), their speed dependence components $\gamma_2$ ($\Gamma_2/P$, in $cm^{-1}atm^{-1}$) and $\delta_2$ ($\Delta_2/P$, in $cm^{-1}atm^{-1}$), the Dicke narrowing parameter $\beta$ ($\nu_{vc}$/P, in $cm^{-1}atm^{-1}$) and the first-order line-mixing coefficient $\zeta$ ($Y/P$, in $atm^{-1}$) are globally fitted for each temperature. The mixing ratio of $CO_2$, $X_{CO2}$, is fixed to the value of 398.9 ppm given by the gas supplier. The Doppler width is fixed to its calculated value at the measured temperature and the line intensity, $S$, and the linear baseline are fitted independently for each spectrum. As shown on **Figure 2** for the R(6) transition at 250 K, residuals at the noise level (which is typically $5\times10^{-11}$ $cm^{-1}$ in this case) are achieved using the multi-spectrum fit procedure and SDNGP+LM. This leads to quality factors between 7700 and 14300 in this case ($QF$ is defined as the ratio of the absorption at the peak to the *rms* of the residuals).

It is important to mention that, during the fit procedure, the absorption due to the weak $CO_2$ lines in the neighbourhood of the fitted transition is taken into account by the *MATS* program based on the HITRAN2020 database [16] using a Voigt profile and $X_{CO2}$=398.9 ppm. If significant, absorption due to the interfering water vapour transitions is also calculated and included in the simulation, using the same database and a concentration fixed to a value deduced from isolated $H_2O$ lines. Water vapour mixing ratios were found to be lower than 140 ppm.

The parameter values of this multi-spectrum fit procedure are provided in Supplementary Material for each transition at the different temperatures.

### 3.2. *Temperature dependence of the line parameters*

The multi-spectrum fit procedure applied to the five transitions provides sets of spectroscopic parameters for five temperatures between 250 and 320 K. The temperature dependence of the line parameters can be empirically modelled using the usual power law of the form: $A(T) = A(T_{ref})\left({T_{ref}}/{T}\right)^{n_A}$ where $T_{ref}$ = 296 K, $A(T)$ corresponds to either $\gamma_0$, $\gamma_2$, $\beta$ or $\zeta$ and $n_A$ is the corresponding temperature dependence exponent. In the case of the pressure shift and its speed dependence component ($\delta_2$), the following linear dependence is applied: $\delta_i(T) = \delta_i(T_{ref}) + \delta_i'(T - T_{ref})$ (with $i$= 0 or 2) to allow for a change of sign for $\delta_i$. Note that since we are working with a mixture of $CO_2$ at a very low mixing ratio in air ($X_{CO2}$=398.9 ppm), the contribution due to collisions between two $CO_2$ molecules can be neglected for all parameters. For example, as $\gamma_0(T) = \gamma_{self}(T)X_{CO_2}P_{tot} + \gamma_{air}(T)(1 - X_{CO_2})P_{tot}$, $\gamma_0$ can be assimilated to $\gamma_{air}$ with a relative error smaller than $1.5\times10^{-4}$.

Plotting the retrieved parameters $\gamma_0(T)$, $\beta(T)$ and $\zeta(T)$ *versus* $T_{ref}/T$ and fitting these data points with a function of the form $y = ax^b$, allows determining $A(T_{ref})$ and $n_A$. In the same way, $\delta_0(T)$ is plotted *versus* $(T-T_{ref})$ to retrieve $\delta_0(T_{ref})$ and $\delta_0'$. In the case of $\gamma_2(T)$ the things are slightly different, as in the *MATS* program the fit output corresponds to $a_w = \frac{\gamma_2(T)}{\gamma_0(T_{ref})}$ because no temperature dependence is assumed *a priori* ($n_{\gamma_2} = 0$). Hence, by plotting $a_w(T)$ *versus* $T_{ref}/T$ and fitting these data points with a function of the form $y=ax^b$ we obtain $a_w(T_{ref}) = \gamma_2(T_{ref})/\gamma_0(T_{ref})$ and $n_{\gamma_2}$. In the case of $\delta_2(T)$, the fit output corresponds to $a_s = \frac{\delta_2(T)}{\delta_0(T_{ref})}$. By plotting $a_s$ *versus* $(T-T_{ref})$, we obtain $a_s(T_{ref}) = \delta_2(T_{ref})/\delta_0(T_{ref})$ and $\delta_2'$.

The different parameters obtained from the multi-spectrum fit procedure are plotted *versus* temperature on **Figure 3**. The retrieved parameter values at $T_{ref}$ and their temperature dependence coefficients are given in **Table 2** and compared with the most accurate literature data in the next section. Note that in the fits on **Figure 3**, the data are weighted by the inverse of the squared uncertainty estimated as discussed below.

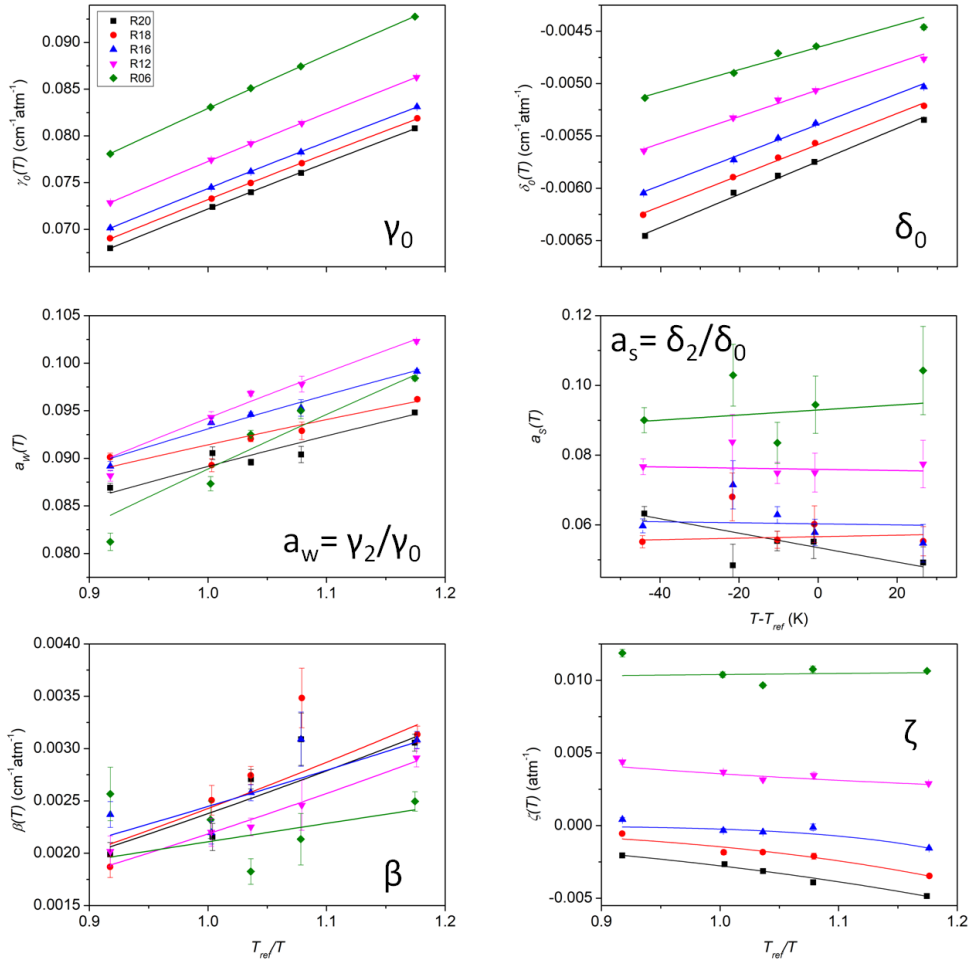


*Figure 3. Variation of the fitted parameters of the R(6), R(12), R(16), R(18) and R(20) lines of the 30013-00001 band of $^{12}CO_2$ versus the temperature. The parameters $\gamma_0$, $\beta$, $a_w$, $\zeta$ are fitted with a function of the form $y = ax^b$ to*

229 *determine their value at $T_{ref}$ and the temperature dependence exponent. The $\delta_0$ and $a_s$ parameters are fitted*
230 *with a linear function which provides their value at $T_{ref}$ and the temperature dependence coefficient (see text).*

231

| | $\gamma_0$ | $n_{\gamma 0}$ | $\delta_0$ | $\delta'$ | $\beta$ | $n_\beta$ | $a_w$ | $n_{\gamma 2}$ | $a_s$* | $\zeta$ | $n_\zeta$ |
|---|---|---|---|---|---|---|---|---|---|---|---|
| | $cm^{-1}atm^{-1}$ | | $cm^{-1}atm^{-1}$ | $cm^{-1}atm^{-1}K^{-1}$ | $cm^{-1}atm^{-1}$ | | | | | $atm^{-1}$ | |
| **R(6)** | 0.08295(3) | 0.698(4) | -0.00465(3) | 0.0000107(10) | 0.00211(22) | 0.8(9) | 0.0889(12) | 0.66(10) | 0.093(5) | 0.01040(49) | 0.1(4) |
| **R(12)** | 0.07726(1) | 0.682(2) | -0.00506(2) | 0.0000128(7) | 0.00218(5) | 1.7(2) | 0.0942(6) | 0.52(5) | 0.076(2) | 0.00357(15) | -1.4(4) |
| **R(16)** | 0.07437(1) | 0.683(2) | -0.00539(1) | 0.0000146(5) | 0.00245(10) | 1.4(4) | 0.0931(3) | 0.39(3) | 0.060(3) | -0.00024(12) | 11.5(32) |
| **R(18)** | 0.07318(3) | 0.687(4) | -0.00558(1) | 0.0000148(5) | 0.00243(13) | 1.8(5) | 0.0914(5) | 0.30(5) | 0.057(2) | -0.00146(13) | 5.4(6) |
| **R(20)** | 0.07218(2) | 0.699(3) | -0.00574(2) | 0.0000158(6) | 0.00238(11) | 1.7(4) | 0.0892(5) | 0.37(4) | 0.054(2) | -0.00277(6) | 3.5(2) |

*Note*

** These values correspond to the mean value averaged over all the temperatures.*

*Table 2. List of the spectroscopic parameters obtained for the five transitions studied in this work. A SDNG profile is used in the multi-spectrum fit procedure. One-sigma uncertainties are given in parenthesis in the unit of the last digit. Here, $a_w$ and $a_s$ correspond to $\gamma_2/\gamma_0$ and $\delta_2/\delta_0$, respectively.*

### *3.3 Estimated error budget*

#### *a. Type-A uncertainty*

As explained in [26], the standard error provided for each fitted parameter by the *MATS* program could underestimate the « real error » by factors between typically 3 to 5, depending of the considered parameter, because the numerical correlations between the parameters are not taken into account in the calculation of this standard error. To estimate these factors in our case, we first simulated 100 spectra with different random noise and then calculated the standard deviation of the fitted parameters. In our typical noise conditions (10 kHz or $\sigma_x$= 3×10$^{-3}$% of the Doppler FWHM on the *x*-axis and 1×10$^{-10}$ cm$^{-1}$ or $\sigma_y$= 0.02% of the maximum absorption on the *y*-axis), we found that the uncertainty reported for the fitted parameters is equivalent to the « real error » showing that the impact of the correlation between the parameters is small thanks to the low noise level on the two axis. The fit errors are thus directly considered as our type-A uncertainty.

#### *b. Type-B uncertainty*

To evaluate possible biases due to inaccurate pressure and temperature values, we also adopted the method described in [26] consisting, for a given transition and temperature, in: *(i)* generating a set of spectra at the five pressures of the recordings using our list of spectroscopic parameters and a SDNG profile and fixing one parameter (the temperature or the total pressure in our case) to its biased value and, then *(ii)* fitting these simulated spectra with the « true » temperature or total pressure. The retrieved spectroscopic parameters are then compared to the values used to generate the spectra. Here we adopted a bias of 0.1% for the total pressure, corresponding to the uncertainty of the pressure gauge, and a bias of 0.1 K for the temperature reflecting the uncertainty on the absolute temperature measurement and the inhomogeneity of the sounded gas temperature [20]. At 274 K a bias of 0.3 K is applied due to the larger temperature inhomogeneity of the V1 cell. These evaluations have been done for all the transitions and temperatures. Note that a bias related to $X_{CO2}$ was not considered here as this parameter (in fact the line intensity which is equivalent) was fitted for each spectrum.

Final uncertainties on the spectroscopic parameters retrieved from the multi-spectrum fit procedure at temperature *T* are then calculated as the square root of the quadratic sum of the type-A and type-B errors. These 1$\sigma$-uncertainties are plotted in **Figure 3**. By looking to these plots, we can observe that the estimated final uncertainties are consistent with the dispersion of the parameter values, the fitted curves being within a ±2$\sigma$ interval in most of the cases. We nevertheless note that, for some transitions, the final uncertainties seem to be underestimated by a factor of ~2 for the $\delta_0$, $a_w$ and $\zeta$ parameters at 285 and 320 K and for the $\beta$ parameter of the R(6) transition.

The uncertainties included in **Table 2** for the spectroscopic parameters at $T_{ref}$= 296 K and their temperature dependence exponent, correspond to the fit error taking into account the uncertainties on the spectroscopic parameters at each temperature.

## 4. Discussion

As mentioned above, a number of previous spectroscopic works have already been reported for the $^{12}CO_2$ band studied here. We will limit our discussion to:

*(i)* The FTS measurements by Devi et al. [1] (also named hereafter Devi2016), whose results, obtained with a quadratic speed-dependent Voigt profile including line-mixing, are implemented in the latest version (5.1) of the absorption coefficient (ABSCO) tables for the Orbiting Carbon Observatories for the 1.6 μm band [27],

*(ii)* The latest version of the HITRAN database (HITRAN2020) [16] which is based on empirical modeling described in Ref. [18], adopting as in Ref. [1] a quadratic speed-dependent Voigt profile with line-mixing,

*(iii)* The rCMDS calculations [19] (also named hereafter Nguyen2020) which provides Voigt and non-Voigt line-shape parameters to complement the databases when no experimental data are available. Note that the rCMDS spectroscopic parameters are only given for the P-branch, but Nguyen et al. indicated that *the calculated R branch spectrum will be the exact symmetric of the P branch* that we interpret as *the rCMDS spectroscopic parameters are function of the absolute value of m where m=-J and J+1 for the P- and R-branch, respectively* [19].

*(iv)* The Frequency-stabilized (FS)-CRDS measurements on the R(16) transition of the studied band done at NIST between 240 and 290K using a SDNG profile (also named hereafter Ghysels2017) [7].

Recently, several CRDS studies have reported highly accurate measurements (at the kHz level or below) of the positions of the studied $CO_2$ transitions by saturation spectroscopy [6] or from Doppler limited spectra [4,5]. The comparison of our fitted positions with the values provided by these studies shows averaged differences (over the 5 transitions) from 25 kHz at 250K and 285 K, for which the best signal-to-noise ratios are achieved, to 150 kHz in the worst case at 320 K. Fixing the positions to these very accurate values during the multi-spectrum fit procedure modifies only marginally the values retrieved for the different line-shape parameters.

### *a. Comparison of the air-broadening coefficients and their temperature dependence*

Comparison of the retrieved air-broadening coefficients, $\gamma_0(T_{ref})$, with Devi et al, HITRAN and rCMDS values is presented in the upper panel of **Figure 4**. As already observed in [18], rCMDS values are systematically lower than measurements with differences of up to 2.6% compared to our values. Let us remind, that in the rCMDS calculations, the molecules were considered as rigid rotors so that all the effects of vibrational motion were disregarded. In fact, as shown in Fig. 6 of [28], the air-

broadening coefficients at 296 K increase with the vibrational excitation up to few percent's. Due to the underestimation of the rCMDS values, HITRAN2020 adopted rCMDS values for the air-broadening coefficients of $CO_2$ [18] after a rescaling according to the FTS values of Devi et al.. In the lower panel of **Figure 4**, we present the ratios of the experimental air-broadening coefficients to the corresponding HITRAN2020 values. The agreement of our values with HITRAN2020 values is within the HITRAN error bars (*i.e.* 1%) with differences from ~0.1% for R(6) line to 0.85% for the R(16), R(18) and R(20) lines. Interestingly, a systematic difference by about 0.5 % is noted between the P- and R-branches for the FTS values of Devi et al. This difference is between one and two orders of magnitude larger than the experimental error bars of Devi et al. The same behavior is observed for the 30012-00001 band from the data reported in [29]. If confirmed, it would indicate that a universal law in $|m|$, as adopted in the HITRAN list for the air-broadening coefficients, is not adequate to accurately account for the rotational dependence of the air-broadening coefficient in $CO_2$.

Air-broadening coefficients obtained in this work in the R-branch and by Devi et al. are close to each other (**Figure 4**) with differences from -0.18% for the R(18) transition to +0.39% for the R(6) transition. Nevertheless, for this latter transition, the particular FTS value seems to be ~0.3% smaller than what could be extrapolated from the higher *J* lines of the R branch.

It is interesting to consider the impact of the line profile on the derived $\gamma_0$ values in particular because Devi et al. adopted a SDV profile to model their FTS data while a SDNG profile was found necessary to reproduce our CRDS spectra (see **Figure 2**). Following what has been done above to quantify the temperature and pressure biases, we ran our fitting program with a SDV profile instead of a SDNG profile. The $\gamma_{0\_SDV}$ fitted values were found systematically higher than our $\gamma_{0\_SDNG}$ values by 0.15 to 0.17%, thus compensating a significant part of the observed deviations (except for the R(6) transition).

Another possible difference is related to the presence of argon in the air sample used for the measurements. The dry air sample used by Devi et al corresponds to *Ultra Zero grade* from Airgas which is a synthetic blend of 20-22% of oxygen and nitrogen, as found in the supplier documentation, without 1% of argon contrary to our air sample. To evaluate the impact of argon, we used the results of Ref. [29] where the $O_2$-, $N_2$- and Ar-broadening coefficients are measured for the nearby 30012-00001 $CO_2$ band by frequency-agile rapid scanning (FARS) CRDS technique. Replacing 1% of $N_2$ by 1% of Ar leads to a decrease of the broadening coefficient by ~0.2%. Note that the exact $O_2$ mixing ratio in the mixture used by Devi et al. is not given and could also have an effect on the reported broadening coefficients.

After correction of the FTS data from these two effects, the differences are reduced to less than 0.2% for the R(10), R(16), R(18) and R(20) transitions, the deviation of the R(6) "outlier" reaching a value of 0.7%.

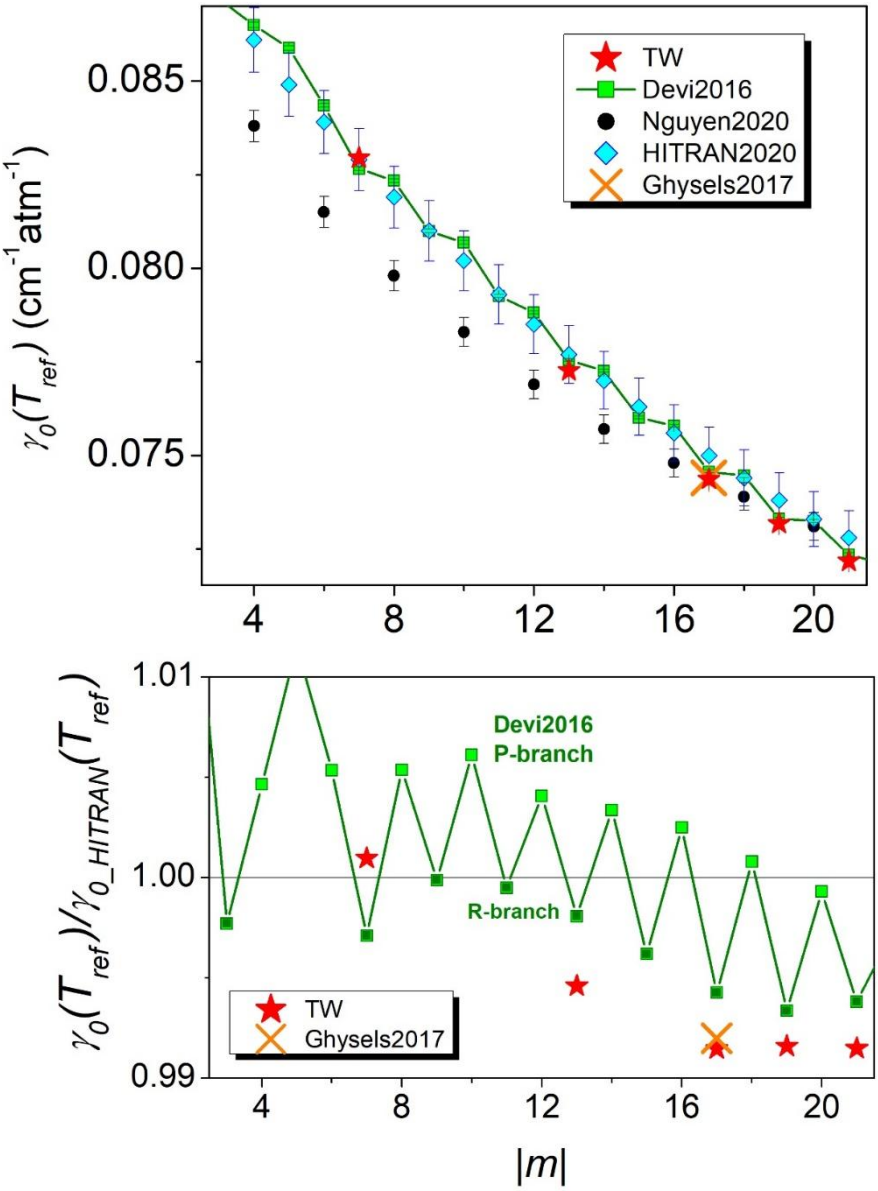


*Figure 4. Comparison of the retrieved air-broadening coefficients, $\gamma_0(T_{ref})$, with a selection of recent works: Devi2016 [1], Nguyen2020 [19], Ghysels2017 [7] and HITRAN2020 [16] (Upper panel). Ratios of the air-broadening coefficients obtained in this work (TW), in Devi2016 and in Ghysels2017 to those of HITRAN2020 are presented in the lower panel. A 1%-uncertainty is reported for HITRAN2020 values. Note the weak asymmetric behavior between the P- and R-branch.*

We have included in Fig. 4, the NIST value for the R(16) transition [7] obtained for 400 ppm of $CO_2$ in purified dry air (thus containing argon as in our sample) using a SDNG profile. An excellent agreement is achieved (difference of about 0.04%).

From this discussion, we conclude that accuracy on the $\gamma_0$ determination at the 0.1% level requires to carefully consider the impact of the line profile and the composition of the dry air sample (fraction of $O_2$ and $N_2$, presence of argon).

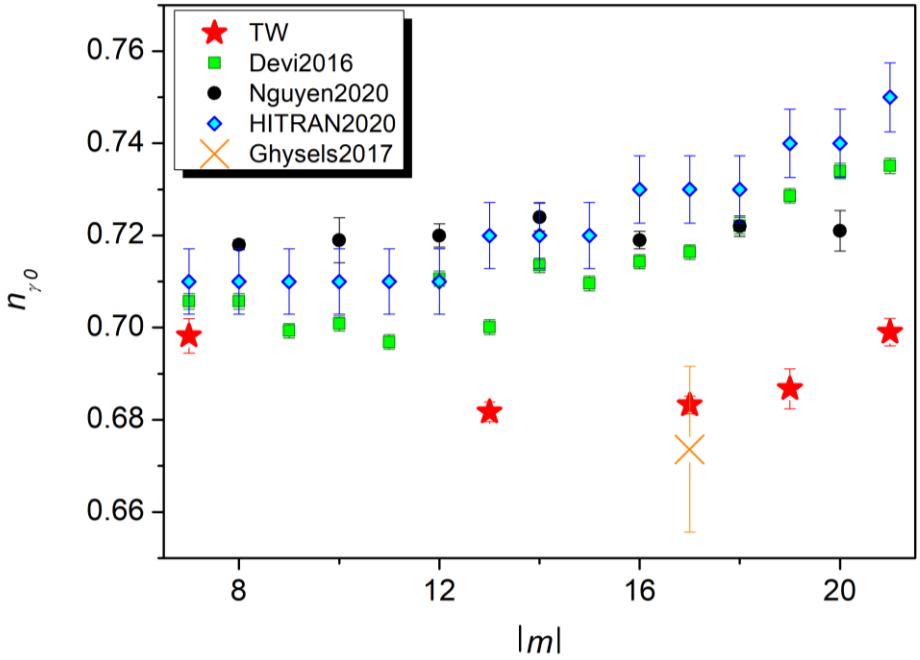


*Figure 5. Comparison of the retrieved temperature dependence exponent of the air-broadening coefficient, $n_{\gamma_0}$, with a selection of recent works: Devi2016 [1], Nguyen2020 [19], Ghysels2017 [7] and HITRAN2020 [16].*

The $\gamma_0$ temperature dependence exponent obtained in the present work shows a clear $m$ dependence contrary to the rCMDS calculated values which are almost constant for $|m|>5$ (see **Fig. 5**). The rCMDS values are systematically higher by 2.5 to 6% which can be considered as satisfactory for these calculations [19]. The comparison with Devi et al gives differences on the same order. As rCMDS calculations of $n_{\gamma_0}$ for air and $O_2$ show that $n_{\gamma_0}$ is not very sensitive to the perturber [19], the observed deviations cannot be due to the presence of 1% of argon in our air mixture. The observed differences are possibly explained by the use of different line profiles (*i.e.* SDNG profile in this work and a SDV profile in Devi et al.).

For the R(16) transition we see that the NIST $n_{\gamma_0}$ value [7] obtained with a SDNG profile agrees with our value. In the same paper, the $n_{\gamma_0}$ value retrieved from a SDV profile was found in very good agreement with the value reported in Devi et al. which might indicate that temperature dependence exponent of the air-broadening coefficient is quite sensitive to the choice of the profile. The fitting of our spectra with a SDV profile did not confirm this sensitivity, the retrieved $n_{\gamma_0}$ value being almost unchanged when using one or the other profile (including line-mixing effects). Note that NIST estimated uncertainty of 0.018 is about ten times larger than what is estimated for the same

transition in our work (0.002). If we try to fit our $\gamma_0(T)$ data by fixing $n_{\gamma_0}$ to the values reported by Devi et al. (and by freeing $\gamma_0(T_{ref})$), a clear mismatch between the fit and our data is observed with differences up to ±0.4% for the two "extreme" temperatures (250 and 320 K). This shows the importance of an accurate determination of $n_{\gamma_0}$. As HITRAN2020 values are fitted on the FTS data of Devi et al. with Padé approximants, similar differences are observed compared to HITRAN values.

*b. Comparison of the air-pressure shifts and their temperature dependence*

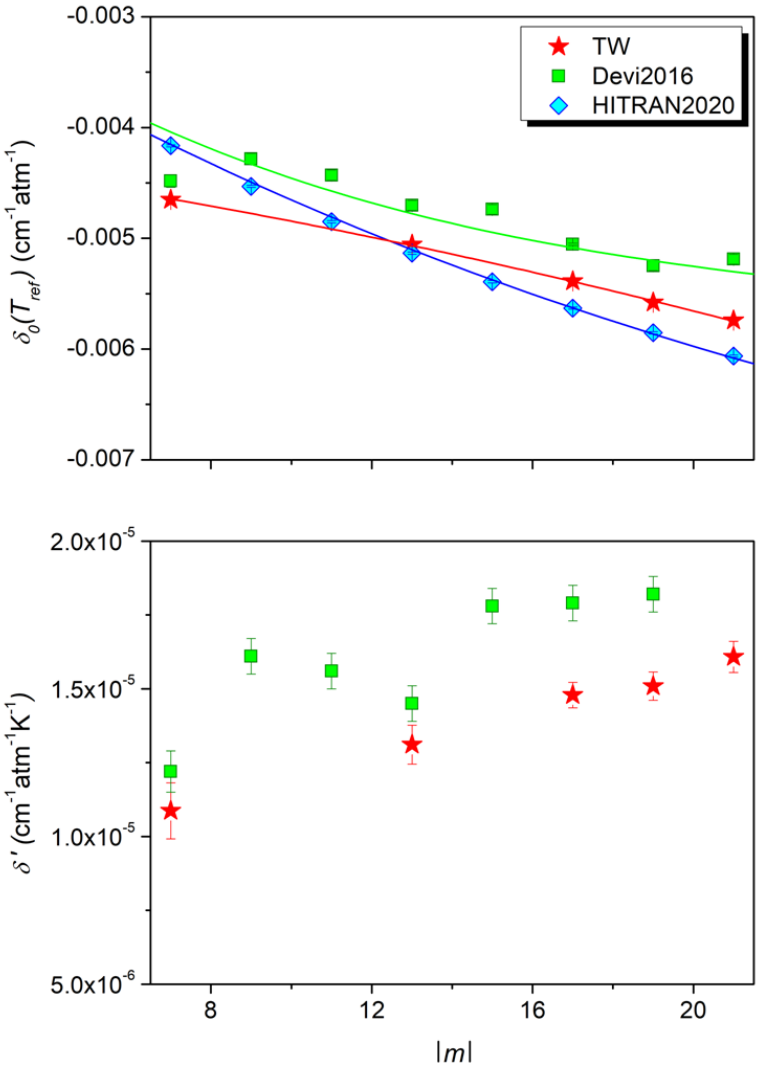


*Figure 6. Comparison of the retrieved air-pressure shift coefficients, $\delta_0(T_{ref})$, (Upper panel) and its temperature dependence coefficients, $\delta'$, with Devi2016 [1] and HITRAN2020 [16]. Note that no temperature dependence is reported in HITRAN2020.*

In HITRAN2020, the approach proposed by Hartmann [30] is adopted to extend to other vibrational bands the air-pressure shift coefficients fitted to one band. The good agreement observed with our data (**Figure 6**) demonstrates the relevance of this approach. Devi et al. pressure shifts are smaller than our values by amounts between 3×10$^{-4}$ and 5.5×10$^{-4}$ cm$^{-1}$atm$^{-1}$ which are outside the

combined error bars. But, the reported FTS error bars (typ. $4.5\times10^{-5}$ $cm^{-1}atm^{-1}$) do not include systematic uncertainties due to wavenumber calibration of the spectra and physical conditions of the spectra. Let us note here that the wavenumber calibration of the FTS spectra recorded by Devi et al was performed using additional absorption cells containing gases (CO, $C_2H_2$ or HCl) for which some transitions have accurately known positions, so that the overall FTS absolute uncertainty on line positions was estimated to be better than ±0.0001 $cm^{-1}$. This uncertainty is a factor of 20 larger than the worst uncertainty on the absolute value of our fitted line positions. Our pressure-shift temperature dependence coefficients are close to the FTS values (although outside the combined error bars) and show an overall smooth increase with $|m|$ (lower panel of **Figure 6**).

*c. Comparison of the Dicke narrowing parameters*

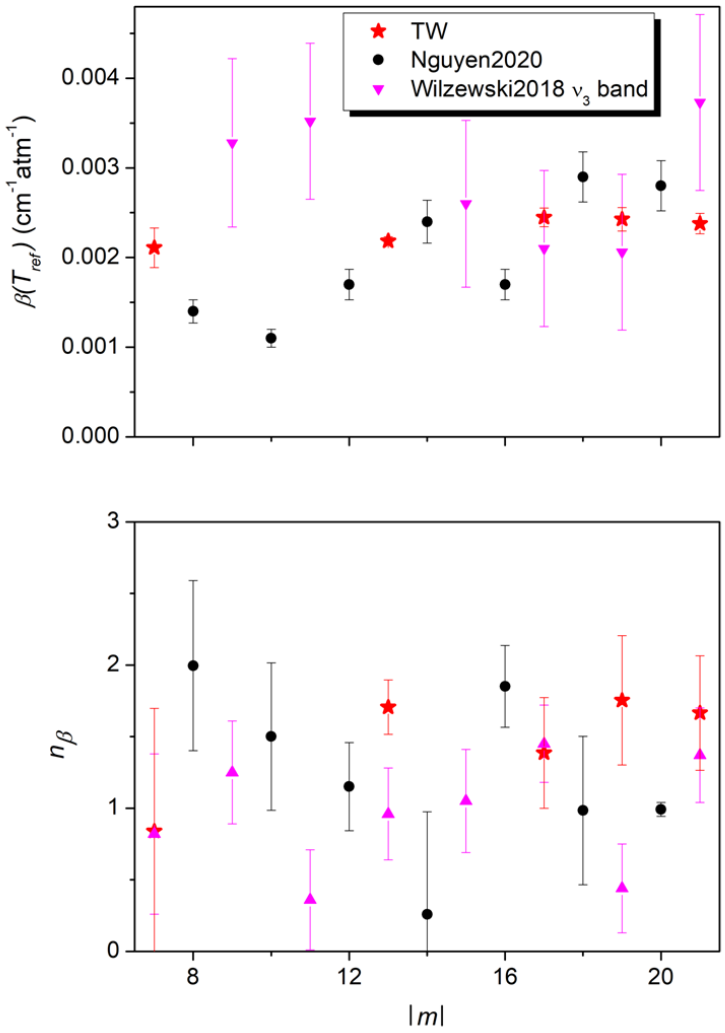


*Figure 7. Comparison of the retrieved Dicke narrowing coefficients, $\beta(T_{ref})$, and of its temperature dependence exponent, $n_\beta$, with a selection of recent works: Nguyen2020 [19] and Wilzewski2018 [31].*

As expected, no evident *m* dependence is observed for $\beta$ and $n_\beta$ (**Figure 7**). With a weighted mean value over *m* of 0.00230(18) $cm^{-1}atm^{-1}$, our Dicke narrowing coefficients are found in good agreement with SDNGP values obtained in Wilzewski2018 [31] for the $\nu_3$ band of $^{12}CO_2$ in $N_2$ and with the rCMDS values [19] (for $CO_2$ in air). Note that these values are quite different from the value of 0.0199 $cm^{-1}atm^{-1}$ obtained from the diffusion coefficient of $CO_2$ in air derived from the kinetic theory of gases [26,32]. The retrieved temperature dependence exponents of the Dicke narrowing coefficients, $n_\beta$, are not accurately determined neither by experiment nor by rCMDS calculations (**Figure 7**) but the different values roughly agree within their large error bars. In our case, the weighted mean value of $n_\beta$ is 1.45±0.32.

*d. The speed-dependent parameters and their temperature dependence*

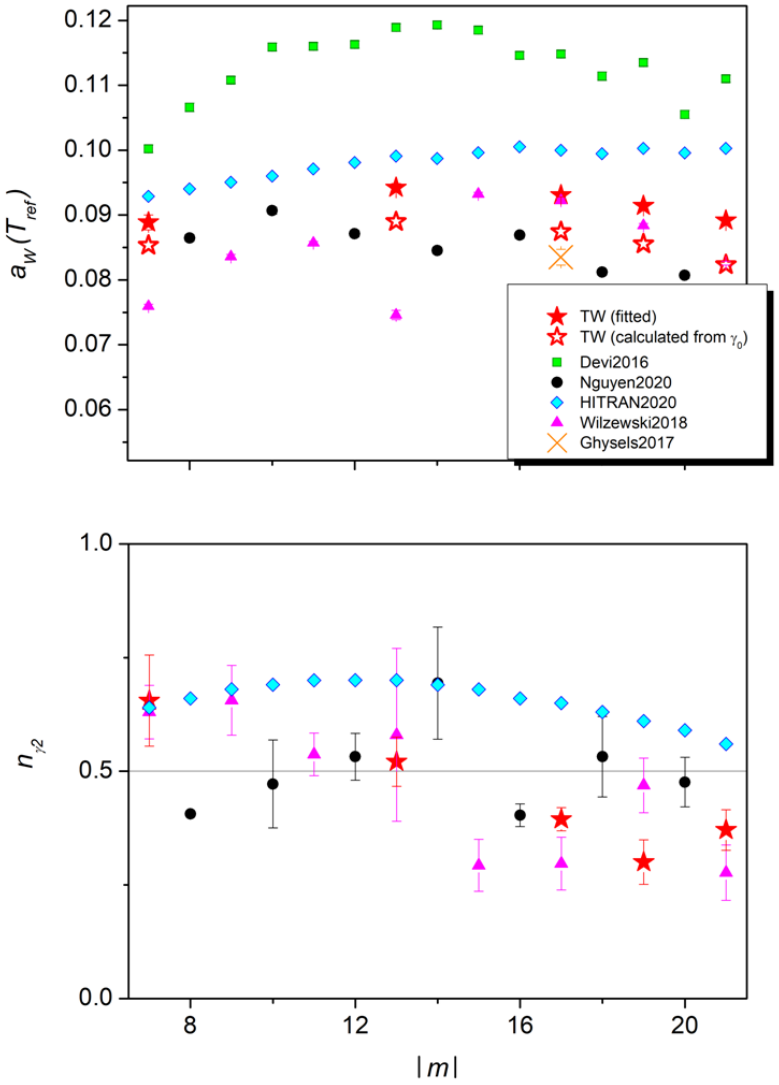


*Figure 8. Comparison of the speed dependent parameter, $a_w(T_{ref})$, and of its temperature dependence exponent, $\boldsymbol{n_{\gamma_2}}$, with a selection of recent works: Devi2016 [1], Nguyen2020 [19], Ghysels2017 [7], Wilzewski2018 [31] and HITRAN2020 [16].*

The $|m|$ dependence of the speed dependent broadening parameter, $a_w(T_{ref})$, is presented in **Figure 8** together with selected literature data. According to Ref. [33], the $a_w(T_{ref})$ values can be computed from the retrieved $\gamma_0(T)$ broadening coefficients and the $m_p/m_a$ mass ratio where $m_p$ and $m_a$ correspond to the mass of the perturber and of the absorber, respectively. The obtained values, included in **Figure 8**, are found consistent with our $a_w(T_{ref})$ values although systematically smaller by 5-7%. Our values are also in good agreement with the rCMDS and HITRAN2020 data and the experimental values of Wilzewski et al. [31] based on a quadratic SDNG profile. Note that the latter study concerns the $\nu_3$ band of $CO_2$ in $N_2$ and not in air. But, by using Ref. [33] to calculate $a_w(T)$, we see that replacing air by $N_2$ decreases $a_w(T_{ref})$ by only 2% for the R(20) transition for example. The $a_w$ value reported by NIST for the R(16) transition is 11.5% lower than our value but this could be explained by the fact that $a_w$ was considered as independent of the temperature [7].

The FTS values of Devi et al. are notably larger than other experimental sources by about 25%. This difference should only be partially explained by the use of a SDV profile instead of a SDNG profile in our work. Indeed, simulations based on the *MATS* program, indicate that, in our conditions, replacing the SDNG profile by a SDV one, leads to an increase of $a_w$ by 5 to 6%. The agreement of Devi et al. is also not very good with the HITRAN2020 data derived from rCMDS using a SDV profile. The difference may also be related to the fact that Devi et al. assumed that $a_w$ is identical for both self- and air-broadening and independent of the gas sample temperature ($\boldsymbol{n_{\gamma_2}} = \mathbf{1}$). This latter assumption is in contradiction with both our results and the experimental results reported by Wilzewski et al. for the $\nu_3$ band (with $\boldsymbol{n_{\gamma_2}}$ on the order of 0.5) (**Figure 8**).

The rCMDS and HITRAN2020 $\boldsymbol{n_{\gamma_2}}$ values (derived from rCMDS calculations fitted with a SDV profile) are in rough agreement with the experimental data. Note that our data and those of Wilzewski et al. seem to show a slow decrease with $|m|$ contrary to rCMDS and HITRAN2020 data.

To our knowledge, no data are available for comparison of $a_s$ (**Table 2**) for which no temperature dependence is detected. A clear decrease with $m$ from 0.093 to 0.053 for $m$= 7 to 21 is obtained for the values averaged over the five temperatures of our measurements.

*e. The line-mixing parameters and their temperature dependence*

Our first-order line mixing parameters at 296 K are plotted on **Figure 9** together with the rCMDS, HITRAN2020 values and the $\nu_3$ results of [31]. The experimental values (relative to different bands) are in close coincidence indicating that there is almost no vibrational dependence. This is confirmed by the rCMDS results (with no vibrational dependence considered) which are systematically smaller but agree satisfactorily with both experimental datasets. The same satisfactory agreement is observed with HITRAN2020 values calculated by Lamouroux et al. [34] using the Energy-Corrected Sudden (ECS) approximation.

447 Devi et al. reported off-diagonal relaxation matrix element coefficients between the nearest
448 neighbor pairs. To convert these matrix element coefficients into the line-mixing parameters plotted
449 on **Figure 9,** we used Eq. IV.24 of [35] and Eq. 7 of [36]. The *m* dependence reported by Devi et al.
450 differs noticeably compared to the experimental values. Devi et al mentioned that *the values of these*
451 *line mixing temperature dependence exponents (…) showed no systematic variations with m or J*
452 contrary to what is shown on **Figure 9**, where the CRDS, FTS and rCMDS temperature dependence
453 exponents, $n_\zeta$, are all in good agreement, showing a clear dependence with *m* with a rapid variation
454 near *m*= 15. To simplify the calculations with HAPI [37], two average values over *m* were adopted for
455 in HITRAN2020 with $n_\zeta = 0.41$ for *m* ≤16 and $n_\zeta = 1.6$ for *m*> 16 [18].

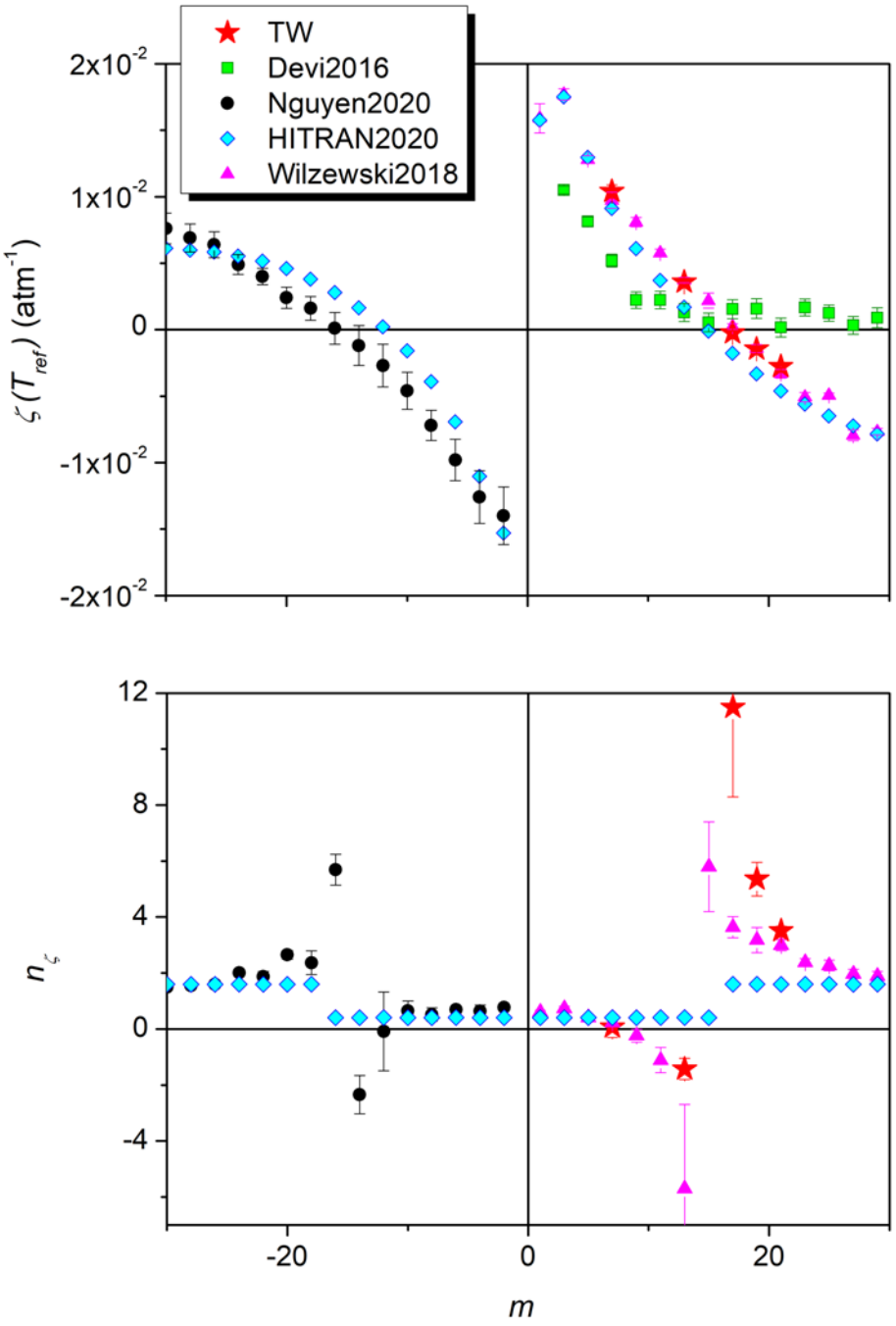


*Figure 9. Comparison of the line-mixing parameter, $\zeta(T_{ref})$, and of its temperature dependence exponent, $n_\zeta$, with a selection of recent works: Devi2016 [1], Nguyen2020 [19], Wilzewski2018 [31] and HITRAN2020 [16].*

## 5. Conclusion

Line-shapes of five transitions of the 30013-00001 band of carbon dioxide have been studied from high sensitivity CRDS spectra recorded with the help of a narrowed and stable (sub-kHz) laser source. Series of spectra were recorded in different conditions of temperature (from 250 to 320 K) and pressure (from 50 to 750 Torr) for a mixture of ~400 ppm of $CO_2$ in air. From a multi-spectrum fit procedure using quadratic SDNG profiles, including the line-mixing effects, the line-shape parameters

were retrieved with reduced uncertainties and limited numerical correlations. Temperature dependence is reported for all of these parameters. Noticeably, contrary to what was claimed in some previous works, a clear temperature dependence is noticed for the speed dependence component of the air-broadening coefficient, very similar to what has been observed in Wilzewski et al. for the $\nu_3$ band of $CO_2$. No temperature dependence is observed for the speed dependence component of the air pressure-shift coefficient. A good overall agreement is obtained with rCMDS data for the different parameters, which participates to the validation of these calculations aiming to fill the databases for the non-Voigt spectroscopic parameters.

A comparison with HITRAN2020 shows that the values reported in this database for the air pressure-broadening and -shift coefficients of the studied transitions are in good agreements with our values. An agreement better than 0.2% is found between the air-pressure-broadening coefficients obtained at 296 K in this work and those from Devi et al., used in the ABSCO tables for the OCO missions, for four of the five transitions studied. Nevertheless, the temperature dependence exponents in Devi et al are systematically higher by up to 6% leading to differences close to 1% for $\gamma_0$ at the lowest atmospheric temperatures. Interestingly, the comparison of our results to the air pressure-broadening available in the literature, in particular the FTS values of Devi et al. and the CRDS values of Adkins et al. [29], revealed a systematic difference by about 0.5 % between the P- and R- branches (**Fig. 4** bottom panel), largely above the experimental uncertainty. The origin of this effect which was apparently not noted in Refs. [1,29], remains unclear but may indicate that the universal law in $|m|$, as adopted in the HITRAN list for the air-broadening coefficients, is not adequate to account for the rotational dependence of the air-broadening coefficient in $CO_2$ at the level of accuracy achieved by the best experiments. Different empirical laws for the P- and R-branches might be required.

**Acknowledgements**

This work is funded by the European Space Agency (ESA) through the contract No. 4000132228/20/I-NS with Deutsches Zentrum fuer Luft- und Raumfahrt) entitled *Improved Spectroscopy for Carbon Dioxide, Oxygen, and Water Vapour Satellite Measurements* for which the authors are sub-contractants. DM wants to thank H. Tran for fruitful discussions on rCMDS results.

495 **References**


[1] Devi VM, Benner DC, Sung K, Brown LR, Crawford TJ, Miller CE, Drouin BJ, Payne VH, Yu S, Smith MAH, Mantz AW, Gamache RR. Line parameters including temperature dependences of self- and air-broadened line shapes of $^{12}C^{16}O_2$: 1.6-µm region. J Quant Spectrosc Radiat Transf 2016;177:117-144. Doi: 10.1016/j.jqsrt.2015.12.020.

[2] Birk M, Röske C, Wagner G. High accuracy $CO_2$ Fourier transform measurements in the range 6000–7000 $cm^{-1}$. J Quant Spectrosc Radiat Transf 2021;272:107791. Doi: 10.1016/j.jqsrt.2021.107791.

[3] Long DA, Truong G-W, Hodges JT, Miller CE. Absolute $^{12}C^{16}O_2$ transition frequencies at the kHz-level from 1.6 to 7.8 µm. J Quant Spectrosc Radiat Transf 2013;130:112-115. Doi : 10.1016/j.jqsrt.2013.07.001.

[4] Reed ZD, Drouin BJ, Long DA, Hodges JT. Molecular transition frequencies of $CO_2$ near 1.6 µm with kHz-level uncertainties. J Quant Spectrosc Radiat Transf 2021; 271:107681. Doi : 10.1016/j.jqsrt.2021.107681.

[5] Reed ZD, Drouin BJ, Hodges JT. Inclusion of the recoil shift in Doppler-broadened measurements of $CO_2$ transition frequencies. J Quant Spectrosc Radiat Transf 2021; 275:107885. Doi : 10.1016/j.jqsrt.2021.107885.

[6] Wu H, Hu C-L, Wang J, Sun YR, Tan Y, Liu A-W, Hu S-M. A well-isolated vibrational state of $CO_2$ verified by near-infrared saturated spectroscopy with kHz accuracy. Phys Chem Chem Phys 2020;22:2841-2848. Doi: 10.1039/C9CP05121J

[7] Ghysels M, Liu Q, Fleisher AJ, Hodges JT. A variable-temperature cavity ring-down spectrometer with application to line shape analysis of $CO_2$ spectra in the 1600 nm region. Appl Phys B 2017;123:124. Doi :10.1007/s00340-017-6686-y

[8] Crisp D, Atlas RM, Breon F-M, Brown LR, Burrows JP, Ciais P, Connor BJ, Doney SC, Fung IY, Jacob DJ, Miller CE, O'Brien D, Pawson S, Randerson JT, Rayner P, Salawitch RJ, Sander SP, Sen B, Stephens GL, Tans PP, Toon GC, Wennberg PO, Wofsy SC, Yung YL, Kuang Z, Chudasama B, Sprague G, Weiss B, Pollock R, Kenyon D, Schroll S. The Orbiting Carbon Observatory (OCO) mission mission. Adv Space Res 2004;34:700–709.Doi: 10.1016/j.asr.2003.08.062.

[9] Crisp D, Miller CE, DeCola PL. NASA Orbiting Carbon Observatory: measuring the column averaged carbon dioxide mole fraction from space. J Appl Rem Sens 2008;2:023508. Doi: 10.1117/ 1.2898457.

[10] Boesch H, Baker D, Connor B, Crisp D, Miller CE. Global characterization of $CO_2$ column retrievals from shortwave-infrared satellite observations of the Orbiting Carbon Obs-2 Mission. Remote Sens 2011;3:270–304. Doi: 10.3390/rs3020270

[11] Eldering A, Taylor TE, O'Dell CW, PavlickR. The OCO-3 mission: measurement objectives and expected performance based on 1 year of simulated data. Atmos Meas Tech 2019;12:2341–2370. Doi: 10.5194/amt-12-2341-2019.

[12] Kuze A, Suto H, Nakajima M, Hamazaki T. Thermal and near infrared sensor for carbon observation Fourier transform spectrometer on the Greenhouse Gases Observing Satellite for greenhouse gases monitoring. Appl Opt 2009;48:6716–33. Doi:10.1364/AO.48.006716.

[13] Miller CE, Crisp D, DeCola PL, Olsen SC, Randerson JT, Michalak AM, Alkhaled A, Rayner P, Jacob DJ, Suntharalingam P, Jones DBA, Denning AS, Nicholls ME, Doney SC, Pawson S, Boesch H, Connor BJ, Fung IY, O'Brien D, Salawitch RJ, Sander SP, Sen B, Tans P, Toon GC, Wennberg PO, Wofsy SC, Yung YL, Law RM.
Precision requirements for space-based $X_{CO2}$ data. J Geophys Res: Atmos 2007;112:D10314. Doi:10.1029/2006JD007659

[14] Hobbs JM, Drouin BJ, Oyafuso F, Payne VH, Gunson MR, McDuffie J, Mlawer EJ. Spectroscopic uncertainty impacts on OCO-2/3 retrievals of $X_{CO2}$. J Quant Spectrosc Radiat Transf 2020;257:107360. Doi: 10.1016/j.jqsrt.2020.107360.

[15] Copernicus CO2 Monitoring Mission Requirements Document, EOP-SM/3088/YM-ymIssue 2.0, 2019. available via https://esamultimedia.esa.int/docs/EarthObservation/CO2M_MRD_v2.0_Issued20190927.pdf

[16] Gordon IE, Rothman LS, Hargreaves RJ, Hashemi R, Karlovets EV, Skinner FM, Conway EK, Hill C, Kochanov RV, Tan Y, Wcisło P, Finenko AA, Nelson K, Bernath PF, Birk M, Boudon V, Campargue A, Chance KV, Coustenis A, Drouin BJ, Flaud J-M, Gamache RR, Hodges JT, Jacquemart D, Mlawer EJ, Nikitin AV, Perevalov VI, Rotger M, Tennyson J, Toon GC, Tran H, Tyuterev VG, Adkins EM, Baker A, Barbe A, Canè E, Császár AG, Dudaryonok A, Egorov O, Fleisher AJ, Fleurbaey H, Foltynowicz A, Furtenbacher T, Harrison JJ, Hartmann J-M, Horneman V-M, Huang X, Karman T, Karns J, Kassi S, Kleiner I, Kofman V, Kwabia–Tchana F, Lavrentieva NN, Lee TJ, Long DA, Lukashevskaya AA, Lyulin OM, Makhnev VY, Matt W, Massie ST, Melosso M, Mikhailenko SN, Mondelain D, Müller HSP, Naumenko OV, Perrin A, Polyansky OL, Raddaoui E, Raston PL, Reed ZD, Rey M, Richard C, Tóbiás R, Sadiek I, Schwenke DW, Starikova E, Sung K, Tamassia F, Tashkun SA, Vander Auwera J, Vasilenko IA, Vigasin

AA, Villanueva GL, Vispoel B, Wagner G, Yachmenev A, Yurchenko SN. The HITRAN2020 molecular spectroscopic database. J Quant Spectrosc Radiat Transf 2022; 277:107949. Doi: 10.1016/j.jqsrt.2021.107949.
[17] Jacquinet-Husson N, Armante R, Scott NA, Chédin A, Crépeau L, Boutammine C, Bouhdaoui A, Crevoisier C, Capelle V, Boonne C, Poulet-Crovisier N, Barbe A, Benner DC, Boudon V, Brown LR, Buldyreva J, Campargue A, Coudert LH, Devi VM, Down MJ, Drouin BJ, Fayt A, Fittschen C, Flaud J-M, Gamache RR, Harrison JJ, Hill C, Hodnebrog Ø, Hu S-M, Jacquemart D, Jolly A, Jiménez E, Lavrentieva NN, Liu A-W, Lodi L, Lyulin OM, Massie ST, Mikhailenko S, Müller HSP, Naumenko OV, Nikitin A, Nielsen CJ, Orphal J, Perevalov VI, Perrin A, Polovtseva E, Predoi-Cross A, Rotger M, Ruth AA, Yu SS, Sung K, Tashkun SA, Tennyson J, Tyuterev VG, Vander Auwera J, Voronin BA, Makie A. The 2015 edition of the GEISA spectroscopic database, J Mol Spectr 2016; 327:31-72. Doi : 10.1016/j.jms.2016.06.007.
[18] Hashemi R, Gordon IE, Tran H, Kochanov RV, Karlovets EV, Tan Y, Lamouroux J, Ngo NH, Rothman LS. Revising the line-shape parameters for air- and self broadened $CO_2$ lines toward a sub-percent accuracy level, J Quant Spectrosc Radiat Transf 2020;256:107283. Doi: 10.1016/j.jqsrt.2020.107283.
[19] Nguyen HT, Ngo NH, Tran H. Line-shape parameters and their temperature dependences predicted from molecular dynamics simulations for $O_2$- and air-broadened $CO_2$ lines. J Quant Spectrosc Radiat Transf 2020;242:106729. Doi: 10.1016/j.jqsrt.2019.106729.
[20] Vasilchenko S, Delahaye T, Kassi S, Campargue A, Tran H, Mondelain D. Temperature dependence of the absorption of the R(6) manifold of the $2v_3$ band of methane in air for the MERLIN mission. Submitted to JQSRT.
[21] Burkart J, Romanini D, Kassi S. Optical feedback stabilized laser tuned by single-sideband modulation. Opt Lett 2013;38:2062-2064. Doi:
[22] Kassi S, Guessoum S, Abanto JCA, Tran H, Campargue A, Mondelain D. Temperature dependence of the collision-induced absorption band of $O_2$ near 1.27 µm. J Geophys Res Atm 2021;126:e2021JD034860. Doi : 10.1029/2021JD034860.
[23] https://github.com/usnistgov/MATS. Doi:10.18434/M32200
[24] Tran H, Ngo NH, Hartmann J-M. Efficient computation of some speed-dependent isolated line profiles.
J Quant Spectrosc Radiat Transf 2013;129:199-20. Doi :10.1016/j.jqsrt.2013.06.015.
[25] Rosenkranz PK. Shape of the 5 µm oxygen band in the atmosphere. IEEE Trans Antennas Propag 1975;23:498–506.
[26] Adkins EM, Hodges JT. Assessment of the precision, bias and numerical correlation of fitted parameters obtained by multi-spectrum fits of the Hartmann-Tran line profile to simulated absorption spectra,
J Quant Spectrosc Radiat Transf 2022;280:108100. Doi: 10.1016/j.jqsrt.2022.108100.
[27] Payne VH, Drouin BJ, Oyafuso F, Kuai L, Fisher BM, Sung K, Nemchick D, Crawford TJ, Smyth M, Crisp D, Adkins E, Hodges JT, Long DA, Mlawer EJ, Merrelli A, Lunny E, O'Dell CW. Absorption coefficient (ABSCO) tables for the Orbiting Carbon Observatories: Version 5.1. J Quant Spectrosc Radiat Transf 2020;255:107217. Doi : 10.1016/j.jqsrt.2020.107217.
[28] Gamache RR, Lamouroux J. The vibrational dependence of half-widths of $CO_2$ transitions broadened by $N_2$, $O_2$, air, and $CO_2$. J Quant Spectrosc Radiat Transf 2013;117:93-103. Doi: 10.1016/j.jqsrt.2012.10.028.
[29] Adkins EM, Long DA, Hodges JT. Air-broadening in near-infrared carbon dioxide line shapes: Quantifying contributions from $O_2$, $N_2$, and Ar. J Quant Spectrosc Radiat Transf 2021;270:107669. Doi: 10.1016/j.jqsrt.2021.107669.
[30] Hartmann J-M. A simple empirical model for the collisional spectral shift of air-broadened $CO_2$ lines. J Quant Spectrosc Radiat Transfer 2009;110(18):2019–2026. Doi:10.1016/j.jqsrt.2009.05.016
[31] Wilzewski JS, Birk M, Loos J, Wagner G. Temperature-dependence laws of absorption line shape parameters of the $CO_2$ $\nu_3$ band. J Quant Spectrosc Radiat Transf 2018;206:296-305. Doi: 10.1016/j.jqsrt.2017.11.021.
[32] https://demonstrations.wolfram.com/BinaryDiffusionCoefficientsForGases/
[33] Lisak D, Cygan A, Wcisło P, Ciuryło R. Quadratic speed dependence of collisional broadening and shifting for atmospheric applications. J Quant Spectrosc Radiat Transf 2015; 151:43-48. Doi : 10.1016/j.jqsrt.2014.08.016.
[34] Lamouroux J, Régalia L, Thomas X, Auwera JV, Gamache R, Hartmann J-M. $CO_2$ line-mixing database and software update and its tests in the 2.1 µm and 4.3 µm regions. J Quant Spectrosc Radiat Transfer 2015;151:88–96. Doi:10.1016/ j.jqsrt.2014.09.017.
[35] Hartmann J-M, Boulet C, Robert D, Chapter IV - Collisional line mixing (within clusters of lines), Editor(s): J-M Hartmann, C Boulet, D Robert, Collisional Effects on Molecular Spectra (Second Edition), Elsevier, 2021, Pages 181-289. Doi : 10.1016/B978-0-12-822364-2.00004-0.
[36] Tran H, Flaud J-M, Gabard T, Hase F, von Clarmann T, Camy-Peyret C, Payan S, Hartmann J-M.

Model, software and database for line-mixing effects in the $\nu_3$ and $\nu_4$ bands of $CH_4$ and tests using laboratory and planetary measurements—I: $N_2$ (and air) broadenings and the earth atmosphere. J Quant Spectrosc Radiat Transf 2006;101:284-305. Doi: 10.1016/j.jqsrt.2005.11.020.
[37] Kochanov RV, Gordon IE,. Rothman LS, Wcislo P, Hill C, Wilzewski JS. HITRAN Application Programming Interface (HAPI): A comprehensive approach to working with spectroscopic data J Quant Spectrosc Radiat Transfer 2016;177:15-30. Doi : 10.1016/j.jqsrt.2016.03.005